AGU100 ADVANCING EARTH AND SPACE SCIENCE

Geophysical Research Letters

RESEARCH LETTER
10.1029/2018GL080317

Key Points:
- The 2011 Grímsvötn volcanic plumes disrupted GPS satellite signals
- We infer water vapor to hail evolution through combined GPS signal-to-noise ratio and phase residual analyses
- Hail formation is corroborated by plume modeling and deposit observations

Supporting Information:
- Supporting Information S1

Correspondence to:
R. Grapenthin,
rg@nmt.edu

Citation:
Grapenthin, R., Hreinsdóttir, S., & Van Eaton, A. R. (2018). Volcanic hail detected with GPS: The 2011 eruption of Grímsvötn Volcano, Iceland. *Geophysical Research Letters*, *45*, 12,236–12,243. https://doi.org/10.1029/2018GL080317

Received 6 SEP 2018
Accepted 3 NOV 2018
Accepted article online 9 NOV 2018
Published online 20 NOV 2018

Volcanic Hail Detected With GPS: The 2011 Eruption of Grímsvötn Volcano, Iceland

R. Grapenthin[1], S. Hreinsdóttir[2,3], and A. R. Van Eaton[4]

[1]Department of Earth and Environmental Sciences, New Mexico Tech, Socorro, NM, USA, [2]Institute of Earth Sciences, University of Iceland, Reykjavík, Iceland, [3]Now at GNS Science, Lower Hutt, New Zealand, [4]Cascades Volcano Observatory, U.S. Geological Survey, Vancouver, WA, USA

Abstract Volcanic plumes are challenging to detect and characterize rapidly, but insights into processes such as hail formation or ash aggregation are valuable to hazard forecasts during volcanic crises. Global Navigation Satellite System (GNSS, which includes GPS) signals traveling from satellites to ground receivers can be disturbed by volcanic plumes. To date, two effects aiding plume detection from GNSS observations have been described: (a) ash-rich plumes scatter the signal, lowering the signal-to-noise ratio (SNR), and (b) some plumes refract and thus delay GNSS signals. Using GNSS data from the VEI 4 2011 Grímsvötn eruption, we show that tephra and water contents of plumes distinctly affect SNR and phase residuals. The signals suggest high-altitude freezing of plume water into volcanic hail—corroborated by 1-D modeling and volcanic hail deposits. Combining GNSS SNR and phase residual analyses is valuable for detecting processes that rapidly scrub fine ash out of the atmosphere.

Plain Language Summary Explosive volcanic eruptions eject hazardous volcanic plumes into the atmosphere, threatening aircraft and downwind communities. Rapid detection and characterization of ash clouds are valuable components of volcano monitoring and hazard assessment. We demonstrate that it is possible to distinguish ash-rich from vapor or ice portions of volcanic plumes using Global Navigation Satellite Systems (GNSS, of which GPS is one constellation) data for the 2011 Grímsvötn eruption in Iceland. Our analyses, combined with insights from 1-D plume modeling, corroborate that GNSS phase residuals and signal-to-noise ratios (SNRs) are sensitive to different plume compositions. Ash-laden plumes generally decrease the SNR at high-elevation angles. Water-vapor-rich plumes, on the other hand, have a greater impact on phase residuals. We combine phase residual and SNR observations and demonstrate that this technique can detect condensation or ice formation in different parts of the plume. Our analysis is validated by models of volcanic plume rise and water phase changes and by field observations of volcanic hail deposits. This finding is significant because it provides a new approach for characterizing plume processes that are relevant to the transport of hazardous ash as hail formation scrubs particles out of the atmosphere.

1. Introduction

Powerful explosive volcanic eruptions eject hazardous volcanic plumes into the atmosphere, threatening aircraft and downwind communities. Rapid detection and characterization of ash clouds are valuable components of volcano monitoring and hazard assessment. Volcanic plumes can produce localized, short-term, dynamic atmospheric heterogeneities that can refract, attenuate, and scatter radio signals of Global Navigation Satellite Systems (GNSS, of which the Global Positioning System, GPS, is one constellation). Two effects are notable: (1) signal refraction causes a phase delay, which can induce artificial position offsets in the GNSS time series (Aranzulla et al., 2013; Grapenthin et al., 2013; Houlié, Briole, Nercessian, & Murakami, 2005; Houlié, Briole, Nercessian, Murakami, & Union, 2005), and (2) scattering and attenuation lower the signal-to-noise ratio (SNR) commonly recorded by GNSS receivers (Larson, 2013; Larson et al., 2017; Ohta & Iguchi, 2015). In cases where the radio signal traveling from satellite to receiver traverses a volcanic plume, these observations can be used for rapid plume detection. Real-time application could potentially augment other satellite observations and provide vital information between remote sensing satellite overpasses, which can be hours apart (e.g., Webley et al., 2013). Furthermore, it is possible to extract more detailed information about the nature of the plume itself.

GNSS-based analysis of plumes for their composition, primarily ash content, is difficult due to their complex makeup. Houlié, Briole, Nercessian, and Murakami (2005) point out that temperature, pressure, and contents of water vapor, other volcanic gases, and solid particles within a volcanic plume can affect the velocity of radio waves. They dismiss volcanic gases (including water vapor) and solid particles as significant sources of disturbance based on results by Solheim et al. (1999) and focus on temperature as the main driver of plume-induced phase delays. However, we suggest that water vapor is important, particularly in the near field, since its effects on GNSS signal refraction have long been recognized and exploited for GNSS meteorology (e.g., Bevis et al., 1992). Furthermore, Solheim et al. (1999) assume a dispersed ash cloud that has been detached from the vent for about 12 hr and contains only small (radius 0.1 – 20 μm), dry particles (based on a study by Wen & Rose, 1994). By contrast, signal effects near the source of the volcanic plume reflect a mixture of hot pyroclasts, magmatic gases (including water vapor), and air. Pyroclasts can range from a few microns to several meters in diameter. Plume water content is determined by several factors, including magma composition, surrounding groundwater, surface water, and atmospheric humidity (Houghton et al., 2015). The importance of these factors is reflected in GNSS analyses of the 2009 eruption of Redoubt Volcano in Alaska where Grapenthin et al. (2013) and Larson (2013) were able to track the plumes for less than an hour, probably because the larger particles ($\gg$ 20μm) and water vapor quickly settled out of the atmosphere by ash aggregation (Van Eaton et al., 2015).

Ohta and Iguchi (2015) report some success in first-order plume analysis with GNSS by applying SNR and phase residual analysis simultaneously to a single vulcanian eruption at Sakurajima Volcano, Japan. They hypothesize that the plume segregated into an ash-rich base and a water-rich top. GNSS phase residual analysis suggests that the water-rich top drifted away from the volcano, while SNR observations show that the ash-rich components remained over the edifice. Unfortunately, clouds obstructed the view and no independent observations exist to substantiate this hypothesis.

Here we demonstrate that it is possible to distinguish ash-rich from vapor- or ice-rich portions of volcanic plumes by analyzing GPS data of the 2011 Grímsvötn eruption in Iceland (Hreinsdóttir et al., 2014; Figure 1a). Our analyses, combined with insights from 1-D plume modeling, confirm that phase residuals and signal-to-noise are sensitive to different plume compositions. We observe altitude-dependent changes in sensitivity of the phase residuals, which can be explained by freezing of water into tephra-laden hail at high altitudes. Both GNSS techniques should be employed in parallel for detection and analysis of volcanic plumes, as either can miss a plume entirely.

2. The 2011 Grímsvötn Eruption

Grímsvötn Volcano is located in the Eastern Volcanic Zone in central Iceland and is the most active volcanic system in Iceland (Figure 1a). The central volcano is covered by the Vatnajökull ice cap. Its ice-filled caldera hosts a subglacial lake with floating ice 200 – 300 m thick (Gudmundsson et al., 2013).

On 21 May 2011, 19:00 UTC, after about 1 hr of precursory seismicity and deformation, Grímsvötn moved into an explosive eruptive phase. Ash plumes reached up to 25 km in altitude, oscillating between 15 and 25 km and slowly declining in altitude until activity waned on 23 May 2011 (Hreinsdóttir et al., 2014). The eruption was observed by the continuous GPS station GFUM located on Mount Grímsfjall, a nunatak protruding the ice at the caldera rim about 6 km east of the vent (Figure 1a). The ice covering the vent melted during the event and formed an ice cauldron about 700 m in diameter (Gudmundsson et al., 2013). The eruption style alternated between wet and dry phases; the wet phases were exclusively fed by the melt water in the ice cauldron (Gudmundsson et al., 2013). A total volume of about 0.7 km^3 (0.27 $\pm$ 0.07 km^3 dense rock equivalent) tephra was produced and during the phreatomagmatic phases external water made up about 20 – 25% of the total plume mass (Gudmundsson et al., 2014; Hreinsdóttir et al., 2014). The plume deposited tephra mostly to the south of the vent (Hreinsdóttir et al., 2014; IMO & IES, 2011) resulting in little to no tephra deposition on the antennas (for ash-on-antenna SNR signal character see Figure 5 in Larson, 2013).

3. Methods and Data

We analyze GPS data from 19 to 22 May 2011 recorded at one sample per second at seven continuous GPS stations around Grímsvötn Volcano (Figure 1a). We focus on the closest site, GFUM; other GPS stations were located more than 40 km away. Legacy GPS transmits on two frequencies: L1 (1575.4 MHz, 0.190 m wavelength) and L2 (1227.6 MHz, 0.244 m wavelength), Misra and Enge (2011) provide full details on GPS

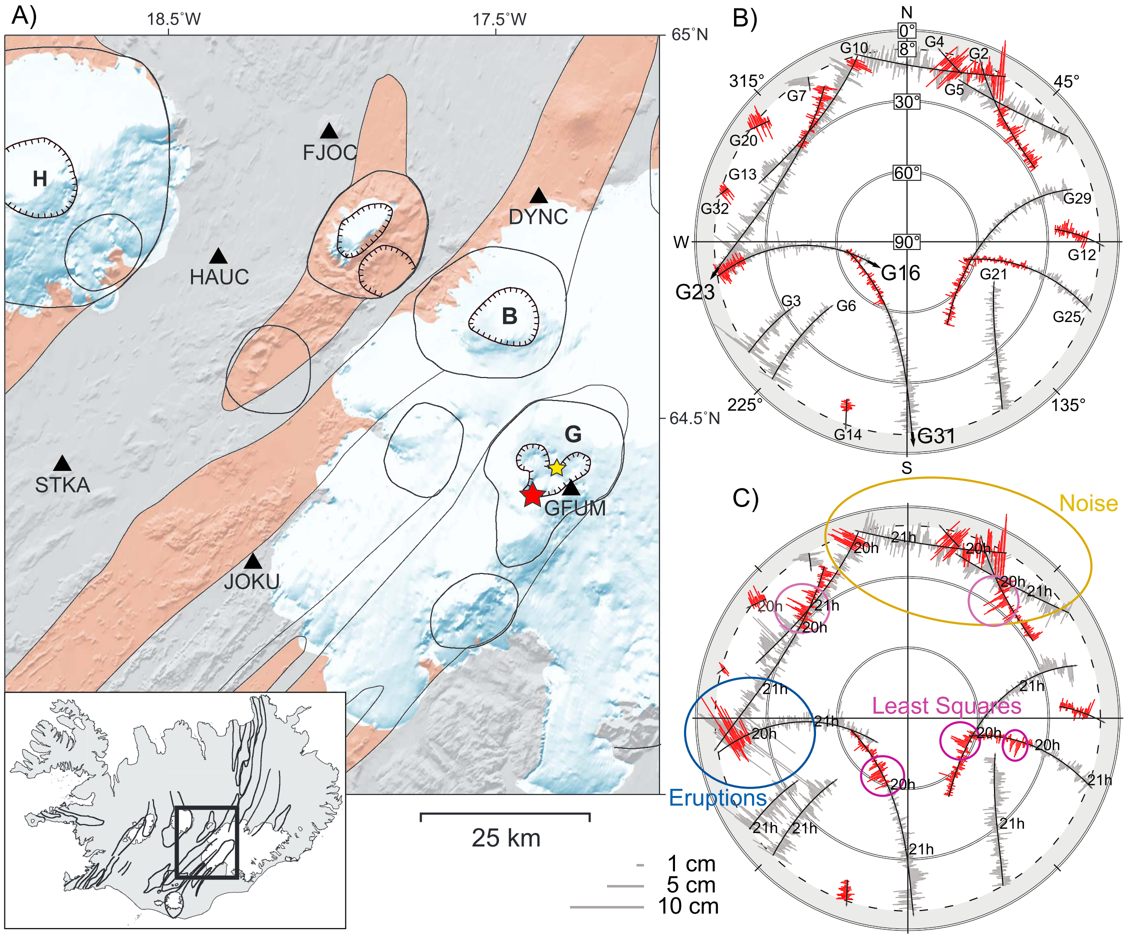

Figure 1. (a) High-rate GPS stations (black triangles) on IS50 base map (Geodetic Survey of Iceland). Volcanic systems (B: Bárðarbunga; G: Grímsvötn; H: Hofsjökull), calderas, and fissure swarms (orange) are from Jóhannesson and Sæmundsson (2009). Grímsvötn caldera with outlines are from Gudmundsson and Milsom (1997). Red star marks vent location; yellow star marks center of magma reservoir (Hreinsdóttir et al., 2014; Sturkell et al., 2003). Inset shows location in Iceland. Skyplots (or azimuth elevation plots) of phase residuals on 20 and 21 May 2011 (red: 19:00-20:00; gray: 20:00-22:00 UTC) along satellite sky tracks on the day before the eruption (b) and during eruption (c). Large phase residuals on both days are due to recurring noise (low-elevation satellites). Phase residuals are positive-up and negative-down in flight direction marked by arrows at tip. (b) Satellite IDs at the tip of skytracks indicate satellite trajectory; bold IDs mark satellites referred to in text and Figure 2. (c) Full UTC hours next to black dots. Blue circle: eruption signals (G16 19:00–20:00; G23 21:00–22:00; red and gray phase residuals, respectively). Brown circle: noise (satellites low in the sky). Magenta circles: artifacts from least squares parameter estimation in positioning solution. See Figure S4 in the supporting information for further analysis.

signals and observables. The analyses presented here are easily expanded to other GNSS constellations and frequencies.

We follow Larson (2013) to determine GPS signal strength, but as the station-vent geometry requires capturing signals propagating low in the sky, we include satellites down to 8° elevation angle. Thus, we suffer from larger surface reflection interference, which has greater impact on low-elevation angle data and results in higher noise (Larson, 2013).

Postfit phase residual values are a by-product of positioning processing and indicate how well the estimated parameters of the positioning solution fit the observations for each satellite. We use NASA JPL's (Jet Propulsion Lab) GIPSY/OASIS II v.6.3 analysis software (Lichten & Border, 1987; Zumberge et al., 1997) with International GNSS Service orbits and antenna phase center models (Dow et al., 2009). We model ocean loading contributions with SPOTL (Agnew, 2012) and apply JPL's ionosphere products to mediate second-order ionosphere effects. The global mapping function and global pressure/temperature models (Boehm et al., 2006, 2007) are applied to treat atmospheric effects.

For the SNR analysis we exclusively use 1 Hz data. Phase residual analysis of longer time periods (> 1 hr) uses 15 s interval observations. To compare sequential days of data, we account for the repeat times of individual

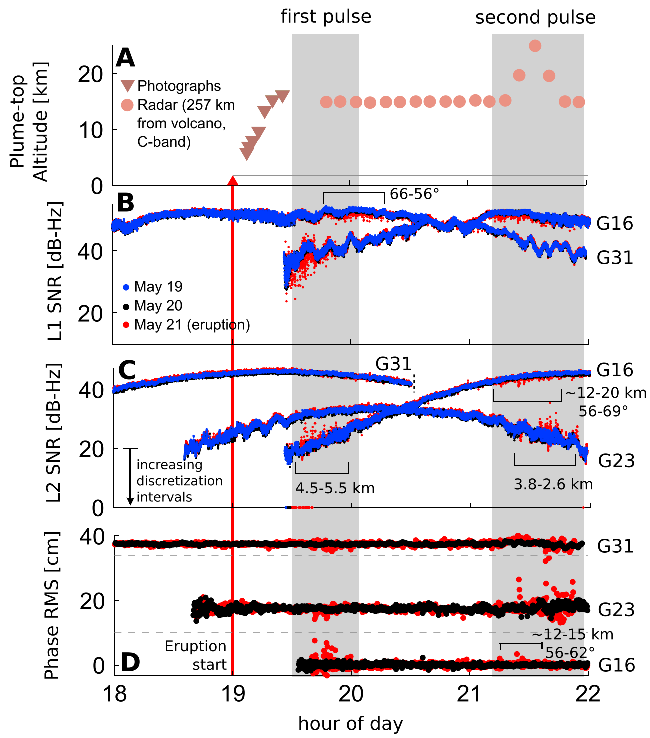

Figure 2. Plume observations from 18:00 to 22:00 UTC at GFUM on 19–21 May 2011. Gray boxes indicate GPS-inferred pulses of explosive activity. (a) Plume-top height from photographs and C-band radar 257 km away from the vent (Petersen et al., 2012). Radar scan intervals over vent are 5 km, hence the flat appearance. Red triangle marks onset of the subaerial eruption; horizontal black line indicates elevation of volcano. (b) L1-SNR on 19–21 May 2011 for satellites G16 and G31 plotted in reverse chronological order (21 May, the day of the eruption, at bottom in red) to highlight differences from noneruptive days (19–20 May). Red line: onset of explosive activity 19:00 UTC on 21 May. SNR increases with satellite elevation angle. (L1 SNR not shown for G23 for clarity.) (c) L2-SNR on satellites G16, G23, and G31. Dashed line terminating G31 indicates that time series was cut short at 20:30 for clarity (compare to Figure 2b). Increase of SNR discretization intervals below 20 db-Hz is marked and visible for G23 and G16; it may default to zero when below 10 db-Hz (likely receiver dependent). (d) Phase residuals for satellites G16 and G23 (shifted for clarity). G16 shows anomalies (red dots below black ones) for the first explosion (G23 anomaly at this time is artifact from GPS processing) and G23 shows anomaly for second explosion, which could be interpreted as two eruptive pulses. SNR = signal-to-noise ratio.

satellites—in general, about 23 hr 56 min. Accordingly, we shift 15 s sample data by 4 min to align 2 days of data. For higher rate data we utilize the exact satellite repeat times (Agnew & Larson, 2007).

To model the properties of the volcanic plume, we use the 1-D model Plumeria (Fortran v. 2.3.1, ; Mastin, 2014). Plumeria solves for the time-integrated, mean flow properties of a volcanic plume assuming a steady state flux of hot pyroclasts, gas, and water vapor into the atmosphere. It considers the effects of water phase changes, crosswinds, and allows the plume to entrain atmospheric moisture or water from the surface. This is important in the case of Grímsvötn due to the large amount of meltwater incorporated. We initialize the model with inputs based on reasonable geologic observations, assuming interaction of basaltic magma (1200 °C) with cold glacial melt water (20% of erupted mass). We use an eruption rate of 8×10^7 kg/s, leading to a plume height of 22 km above sea level (asl), as observed by radar (Arason et al., 2013). The vertical atmospheric profile uses sounding data (temperature, wind speed, and humidity) measured on 22 May 2011 from Keflavík airport 257 km to the west (Figure S1). Supporting information Table S1 provides all input parameters, including a wider range of scenarios to constrain variability in the results.

4. Results and Discussion

4.1. Phase Residuals

In Figures 1b and 1c we show phase residuals plotted along the sky track of each visible satellite from 19:00 to 22:00 UTC on 20 May and the day of the eruption, 21 May 2011 at station GFUM. These plots show satellite tracks in the sky over a GPS antenna, which is located in the center of the plot. In Iceland, satellites in the northern sky (315–45° azimuth) barely achieve 30° elevation angles. The low-elevation causes significant noise, which occurs on both days regardless of eruptive activity (Figures 1b and 1c).

On 20 May, the day before the eruption, satellite G16 presents an initially slightly noisy time series, that becomes very clean at higher-elevation angles (Figure 1b). The following day, however, shows significantly larger phase residuals for G16 during the same time period until about 20:00 UTC (Figure 1c, red spikes inside blue circle; see also Figure 2d). We find another phase residual anomaly at G23 from about 21:25 UTC (single spike) until about 21:40 UTC (Figure 1c, gray spikes inside blue circle; see also Figure 2d) as it sets in the location where G16 rose earlier. Similar to G16, G23 also does not show a phase residual anomaly during this time on the previous day. For both satellites the anomalies emerge when the line of sight between station GFUM and the satellites crosses above the vent (Figure 1a). The supporting information provides further analysis and explain the slight anomalies circled purple in Figure 1c. Importantly, these artifacts, induced by the least squares parameter estimation in the GNSS processing, will spoil phase residual-based 3-D plume tomography.

Since station GFUM is about 6 km east of the vent and we know the satellite elevation angles, we can estimate the heights at which the GPS signals intersect the plume. The signal from G16 pierces the plume from 4.5 to 5.5 km asl (we add 1.8 km elevation at GFUM to calculate asl estimates) above the vent as it rises. The signal with the later anomaly observed by G23 traverses the plume from 3.8 to 2.6 km asl as it sets. Radar, photographic, and visual observations put the top of the initial plume seen by G16 between 15 and 20 km (Figure 2a), while the C-band radar at the airport in Keflavík (257 km from vent with 5 km discretization interval over the volcano) recorded plume heights between 20 and 25 km at the time of G23's anomaly (Figure 2a; Petersen et al., 2012). Notably, G16 is located at high elevation (56–62°) in the direction of the vent when the anomaly is observed at G23. During this time G16's signals should pierce the plume from about 12–20 km asl. Yet G16 shows only small phase residual anomalies during the initial part of the eruption at

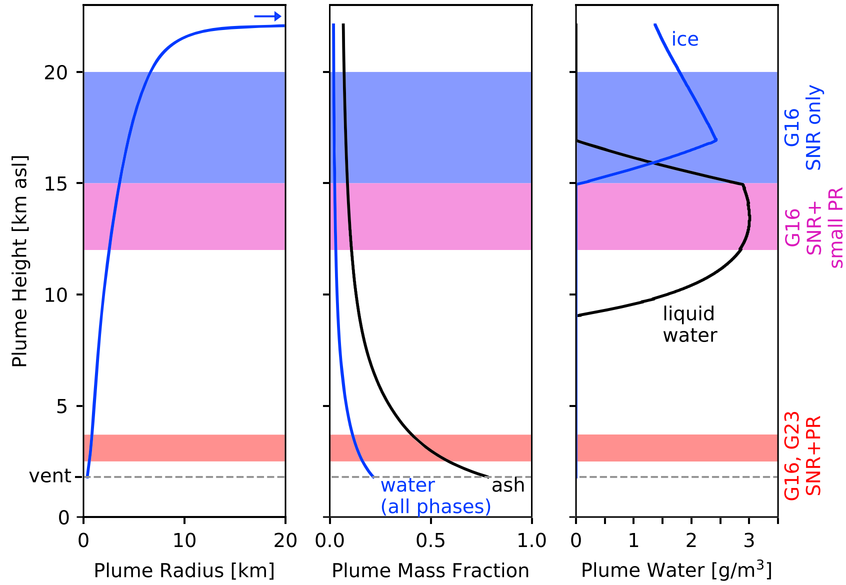

Figure 3. Plume radius, mass fraction, and water concentration results from 1-D volcanic plume model. Horizontal hatched line indicates vent elevation. Plume mass fraction is separated into ash and total water (vapor + liquid + ice). Plume water shows concentration of liquid water and ice. Below 9 km the plume contains water vapor only; by about 16.6 km all water is in the ice phase. Colored background indicates elevations at which signals from satellites G16 and G23 traverse the plume inferred from phase residuals (PRs; notably decreasing toward higher altitudes as water vapor decreases; see Figure 2) and signal-to-noise ratio (SNR).

lower-elevation angles, corresponding to about 12–15 km asl (Figure 2; for lower-elevation angles we use 6 km distance between GFUM and the vent to calculate altitudes; for the higher-elevation angles we use 7 km as a conservative distance estimate to include southward drift of the plume and its finite radius simulated below; at 7 km distance, the range of piercing heights for elevation angles 56–69° is about 12.2–20.0 km).

4.2. SNR and Phase Residual Comparison

We compare phase residuals and SNR observations for the early part of the eruption on 21 May in Figure 2. Beginning at about 19:35, as the GPS signal recorded at station GFUM begins to pierce the plume, SNR on L1 from satellite G16 generally decreases at low-elevation angles, while SNR on L2 increases (Figures 2b and 2c, red dots). This is concurrent with the anomalous phase residuals described above and included in Figure 2d. Neither satellite G23, to the NW, nor satellite G31, at much higher elevation and to the SW of station GFUM, shows L2-SNR anomalies during this time (see Figures 1b and 1c for satellite locations in the sky). However, SNR on L1 from satellite G31 drops significantly at high-elevation angles.

This frequency-dependent difference in behavior can be explained by a transition of the signal path extinction from absorption to scattering (Larson et al., 2017), which occurs on L1 for smaller particles than on L2. Larson et al., (2017, Appendix A) model signal path extinction as a superposition of absorption and scattering for particle diameters much smaller than the radiation wavelength (Rayleigh scattering). Absorption and scattering both depend on the ratio of particle circumference to signal wavelength but raised to the third and sixth power, respectively. If we knew the effective dielectric properties of the scatterers, which are likely aggregates of ash, and water or ice (see below), we could estimate a range of likely particle diameters in the plume at these high altitudes. For instance, if the particles were purely tephra with similar complex dielectric permittivity as used by Larson et al. (2017), particle diameters would range between 6.2 and 13.5 mm. However, this estimate can vary significantly due to the large uncertainties in the scatterer composition and hence the value of the complex dielectric constant.

The second, pulsing anomaly begins at about 21:15 resulting in a clear drop in L1 and L2 SNR for satellite G16 as its signal pierces the plume between 12 and 20 km asl. L2-SNR for satellite G23 increases as the satellite sets (3.8–2.6 km asl). Interestingly, only satellite G23 shows simultaneous extended anomalous phase residuals, while phase residuals for satellite G16 during this time are slightly elevated only for lower-altitude piercing points (about 12–15 km asl; see colored backgrounds in Figure 3).

From field studies of the Grímsvötn eruption deposits, Arason et al. (2013) report layers of ashy volcanic hail. This indicates that water and ice, vaporized from the glacier, turned to liquid in the plume and then froze to create hail (Van Eaton et al., 2015). We hypothesize that the reduction of phase residual anomalies with altitude and their absence at high altitudes during the second eruptive pulse in Figure 1 indicates removal of water vapor and liquid water through freezing and fallout. This phase transition means the GPS signal was not refracted at high altitudes (no phase delay), but was clearly scattered by the hail and tephra (thus lowering the SNR).

4.3. Insights From Plume Modeling

To test our hypothesis that the GPS signals indicate hail formation above 15 km asl, we examined the dynamics of the plume using the 1-D Plumeria model (Mastin, 2014). Model results in Figure 3 show that liquid water begins to condense at about 9 km asl as the plume rises and entrains cooler surrounding air. Then ice begins to nucleate above 14.7 km asl, freezing the majority of liquid water to ice by about 16.6 km asl. These heights corroborate our observations of a marked change in the GPS data above about 15 km asl (Figures 3 and S2). The plume radii we assume when converting elevation angles to piecing heights above are also reasonable based on the model results.

It is important to note that at the short distance that GFUM is away from the vent the choice of distance to the plume has a significant impact on the piercing height estimation, which can change by several kilometers. However, we find that the combination of GPS observations with model results confirms our hypothesis that signal-to-noise ratio and phase residual trade-offs record the transition of water phases in the plume (in this case, removal of liquid water by freezing to ash-laden hail).

4.4. Far-Field Observations

Although the seven remaining stations are between 43 (DYNC) and 100 km (INTA) from the vent (Figure 1a), plume heights between 15 and 25 km could affect signals from satellites at elevation angles below 19–8° for a 15 km plume and 30–14° for a 25 km plume at these distances, respectively.

At these distant stations, satellite G25 recorded at station FJOC and satellite G31 recorded at station DYNC provide some of the few examples of anomalous L2-SNR (L1 is similar) and phase residuals in the direction of the vent (Figure 4). In addition to geometric effects, the reduction in amplitude and duration of the anomalies can likely be explained by wavefront healing, that is, interference of refracted and direct signal. A very subtle drop in SNR and phase residuals (compare Figure 4 to Figure 2), if indeed plume related, suggests that satellite G25 pierces the plume between 20:30 and 20:40 before reaching FJOC. At a vent-station distance of 62 km the piercing height is between 21 and 26 km asl, similar to radar estimates (Hreinsdóttir et al., 2014). Given our previous argument that water refroze to hail for this plume, we suggest that the very small phase residuals at this distance are due to increased residual water in the atmosphere, potentially due elevated ambient temperatures at the top of the umbrella cloud.

Station DYNC, directly north of the vent, records slight phase residual anomalies on satellite G31 from about 21:20–21:45 as it sets in the southern sky. Their interpretation, however, is complicated by an increase in the multipath amplitude (interference between direct and ground-reflected satellite signals) on 20 May, the day before the eruption (Figure 4), suggested by an increase in SNR oscillation amplitude. The larger amplitude of the oscillations indicates improved surface reflectivity due to a smoother surface (e.g., Small et al., 2010), which could be snow. Further snow accumulation could result in the phase shift between 20 May (black dots) and 21 May (red dots; e.g., Larson et al., 2009). We see similar, although not as pronounced changes for other satellites at DYNC. Weather records from the manned weather station Grímsstaðir 100 km north of DYNC show snowfall from 20 May 15:00 to 21 May 09:00 and again from 15:00 to 22 May 18:00 (Þ. Arason, personal communication, October 2016). Given the long duration, snow covering a large region seems justified. The similarity between the phase residual noise on 21 May and 20 May suggests that the peak labeled Plume/Snow? for satellite G31 at station DYNC in Figure 4 is caused by changed multipath due to snow accumulation rather than a plume. However, if the observations at DYNC are plume induced, satellite G31 would have penetrated the plume between about 9.5–12.8 km asl at which we still observe a liquid water phase (Figure 3).

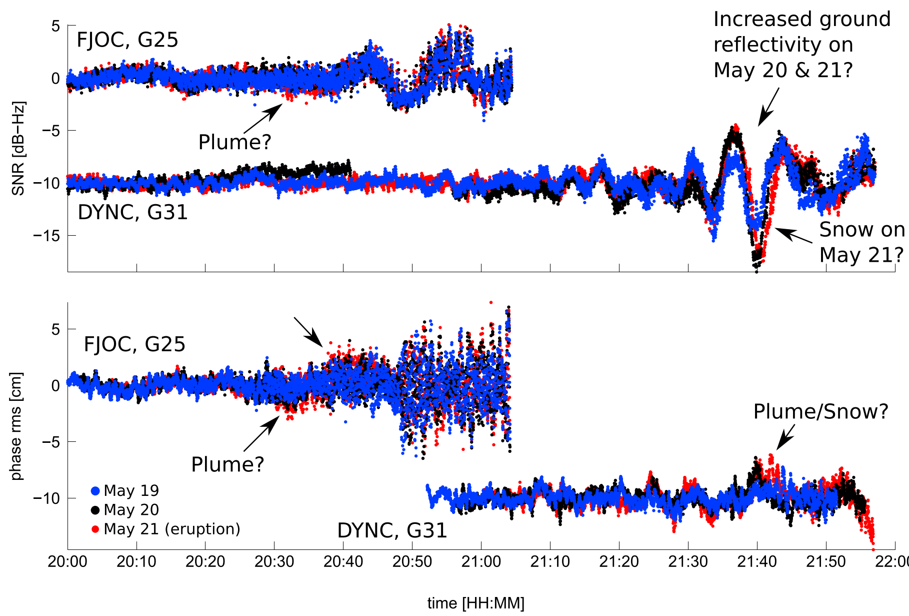

Figure 4. Similar to Figure 2 (detrended SNR) for stations FJOC and DYNC and satellites G25 and G31, respectively. FJOC is 62 km NE of the vent; DYNC is 43 km to the north (Figure 1a). Suspected plume signal in SNR (top) and phase residuals (bottom) are marked for G25 (FJOC). The larger oscillations with phase shifts on G31 (DYNC) after 21:30 indicate snow fall. While a plume signature is missing in the SNR data, it remains unclear whether the peak in phase residuals is related to snow or plume interference. SNR = signal-to-noise ratio.

5. Conclusions

We provide the first high-rate GPS-based plume analysis for an eruption with plume heights of more than 20 km. We combine phase residual and SNR observations for the 2011 Grímsvötn eruption and demonstrate that this technique can detect condensation or ice formation in different parts of the plume. Our analysis is validated by models of volcanic plume rise and water phase changes (Figure 3) and by field observations of volcanic hail in the fall deposits (Arason et al., 2013). Our findings provide a new approach for characterizing plume processes that are relevant to the transport of hazardous ash, because hail formation scrubs particles out of the atmosphere (Van Eaton et al., 2015).

With better knowledge of the effective dielectric properties of ash aggregates and volcanic hail it may be possible to determine particle diameters from multifrequency GNSS SNR observations. This, combined with our observation of water transitioning from vapor to liquid to ice, shows that GNSS can provide valuable near real-time constraints to evaluate tephra dispersion models.

We show that at low satellite elevation angles reflection and interference effects can cause an increase in L2 SNR during interaction with a plume, whereas L1 SNR drops as expected. Although less favorable geometrically and observed with much lower anomaly amplitudes, far-field observations to distances of 40–60 km appear to resolve the uppermost parts of the plumes during the 2011 Grímsvötn eruption.

GNSS is already a common monitoring tool to track deformation at volcanoes. Screening these data for plume signatures can augment the monitoring. While we can detect the highest plumes at Gímsvötn at large distances, near-field observations will provide more reliable results. Azimuthal coverage around the volcano should be considered when designing a GNSS network for plume analysis, and all signals from all available methods on all wavelengths should be analyzed in tandem.

Acknowledgments
The authors thank Þórður Arason (Icelandic Meteorological Office) for the meteorological records at Grímsstaðir and Þorsteinn Jónsson for making sure no GPS data were lost from GFUM during the eruption. Larry Mastin, two anonymous reviewers, and Editor Joel Thornton provided constructive comments that significantly strengthened this study. The data used in this study are available through FUTUREVOLC (http://futurevolc.hi.is). The intermediate TanDEM-X digital elevation model in Figure 1a was provided by the DLR under project IDEM_GEOL0123 to the University of Iceland. The Central Highlands Iceland (CHIL) GPS network was funded by the University of Arizona and grants from NSF (EAR-0711446 to the University of Arizona) and the Icelandic Center for Research RANNIS (60243011 to the Nordic Volcanological Center, University of Iceland). The Grímsvötn GPS station is operated by the Icelandic Meteorological Office with support from the Iceland Glaciological Society, JÖRFI, and the University of Iceland. INTA and KARV were supported by Landsvirkjun, the National Power Company of Iceland, which contributed GPS instruments and seismic sensors north of Vatnajökull. Some figures were made with GMT (Wessel & Smith, 1995).

References

Agnew, D. C. (2012). SPOTL: Some Programs for Ocean-Tide Loading (*Tech. rep.*) La Jolla: Scripps Institution of Oceanography.
Agnew, D. C., & Larson, K. M. (2007). Finding the repeat times of the GPS constellation. *GPS Solutions*, *11*(1), 71–76. https://doi.org/10.1007/s10291-006-0038-4
Aranzulla, M., Cannavò, F., Scollo, S., Puglisi, G., & Immè, G. (2013). Volcanic ash detection by GPS signal. *GPS Solutions*, *17*(4), 485–497. https://doi.org/10.1007/s10291-012-0294-4

Arason, Þ., Þorláksdóttir, B. S., Sigurðsson, G. S., Yeo, R. F., & Thorsteinsson, T. (2013). Properties of ash-infused hail during the Grímsvötn 2011 eruption and implications for radar detection of volcanic columns (Vol. 15, pp. 4797). Vienna, Austria: EGU.

Bevis, M., Businger, S., Herring, T. A., Rocken, C., Anthes, R. A., & Ware, R. H. (1992). GPS meteorology: Remote sensing of atmospheric water vapor using the Global Positioning System. *Journal of Geophysical Research*, *97*(D14), 15,715–787,801.

Boehm, J., Heinkelmann, R., & Schuh, H. (2007). Short note: A global model of pressure and temperature for geodetic applications. *Journal of Geodesy*, *81*, 679–683. https://doi.org/10.1007/s00190-007-0135-3

Boehm, J., Niell, A., Tregoning, P., & Schuh, H. (2006). Global Mapping Function (GMF): A new empirical mapping function based on numerical weather model data. *Geophysical Research Letters*, *33*, L07304. https://doi.org/10.1029/2005GL025546

Dow, J. M., Neilan, R. E., & Rizos, C. (2009). The International GNSS Service in a changing landscape of Global Navigation Satellite Systems. *Journal of Geodesy*, *83*, 191–198. https://doi.org/10.1007/s00190-008-0300-3

Grapenthin, R., Freymueller, J. T., & Kaufman, A. M. (2013). Geodetic observations during the 2009 eruption of Redoubt Volcano, Alaska. *Journal of Volcanology and Geothermal Research*, *259*, 115–132. https://doi.org/10.1016/j.jvolgeores.2012.04.021

Gudmundsson, M. T., & Milsom, J. (1997). Gravity and magnetic studies of the subglacial Grímsvötn volcano, Iceland: Implications for crustal and thermal structure. *Journal of Geophysical Research*, *102*(B4), 7691–7704. https://doi.org/10.1029/96JB03808

Gudmundsson, M., Pálsson, F., Thordarson, T., Höskuldsson, Á., Larsen, G., Högnadóttir, T., et al. (2013). Determining the mass fraction of external water in the plume of the 2011 eruption of Grímsvötn, Iceland. In *EGU General Assembly Conference Abstracts, EGU General Assembly Conference Abstracts*, *15*, pp. 13287.

Gudmundsson, M., Pálsson, F., Thordarson, T., Hoskuldsson, A., Larsen, G., Hognadottir, T., et al. (2014). Water/magma mass fractions in phreatomagmatic eruption plumes—Constraints from the Grímsvötn 2011 eruption. In *AGU Fall Meeting Abstracts*. Abstract V11B-4718.

Houghton, B. F., White, J. D., & Van Eaton, A. R. (2015). *Phreatomagmatic and related eruption styles* (2nd ed.). Amsterdam: Elsevier Inc.537–552 pp., https://doi.org/10.1016/B978-0-12-385938-9.00030-4

Houlié, N., Briole, P., Nercessian, A., & Murakami, M. (2005). Sounding the plume of the 18 August 2000 eruption of Miyakejima Volcano (Japan) using GPS. *Geophysical Research Letters*, *32*, L05302. https://doi.org/10.1029/2004GL021728

Houlié, N., Briole, P., Nercessian, A., Murakami, M., & Union, A. G. (2005). Volcanic plume above Mount St. Helens detected with GPS. *Eos, Transactions American Geophysical Union*, *86*(30), 9–10. https://doi.org/10.1029/2004GL021728.King

Hreinsdóttir, S., Sigmundsson, F., Roberts, M. J., Björnsson, H., Grapenthin, R., Arason, P., et al. (2014). Volcanic plume height correlated with magma-pressure change at Grímsvötn Volcano, Iceland. *Nature Geoscience*, *7*(3), 214–218. https://doi.org/10.1038/ngeo2044

IMO, & IES (2011). Grímsvötn volcano status reports (*Tech. rep.*) University of Iceland: Iceland Meteoroligcal Office and Institute of Earth Sciences.

Jóhannesson, H., & Sæmundsson, K. (2009). Geological map of Iceland. Tectonics.

Larson, K. M. (2013). A new way to detect volcanic plumes. *Geophysical Research Letters*, *40*, 2657–2660. https://doi.org/10.1002/grl.50556

Larson, K. M., Gutmann, E. D., Zavorotny, V. U., Braun, J. J., Williams, M. W., & Nievinski, F. G. (2009). Can we measure snow depth with GPS receivers? *Geophysical Research Letters*, *36*, L17502. https://doi.org/10.1029/2009GL039430

Larson, K. M., Palo, S., Roesler, C., Mattia, M., Bruno, V., Coltelli, M., & Fee, D. (2017). Detection of plumes at Redoubt and Etna volcanoes using the GPS SNR method. *Journal of Volcanology and Geothermal Research*, *344*, 26–39. https://doi.org/10.1016/j.jvolgeores.2017.04.005

Lichten, S. M., & Border, J. S. (1987). Strategies for high-precision Global Positioning System orbit determination. *Journal of Geophysical Research*, *92*(B12), 12,751–12,762. https://doi.org/10.1029/JB092iB12p12751

Mastin, L. G. (2014). Testing the accuracy of a 1-D volcanic plume model in estimating mass eruption rate. *Journal of Geophysical Research: Atmospheres*, *119*, 2474–2495. https://doi.org/10.1002/2013JD020604

Misra, P., & Enge, P. (2011). *Global Positioning System: Signals, measurements and performance* (2nd ed., 569 pp.). Lincoln, MA: Ganga-Jamuna Press.

Ohta, Y., & Iguchi, M. (2015). Advective diffusion of volcanic plume captured by dense GNSS network around Sakurajima volcano: A case study of the vulcanian eruption on July 24, 2012. *Earth, Planets and Space*, *67*(1), 157. https://doi.org/10.1186/s40623-015-0324-x

Petersen, G. N., Bjornsson, H., Arason, P., & von Löwis, S. (2012). Two weather radar time series of the altitude of the volcanic plume during the May 2011 eruption of Grímsvötn, Iceland. *Earth System Science Data Discussions*, *5*(1), 281–299. https://doi.org/10.5194/essdd-5-281-2012

Small, E. E., Larson, K. M., & Braun, J. J. (2010). Sensing vegetation growth with reflected GPS signals. *Geophysical Research Letters*, *37*, L12401. https://doi.org/10.1029/2010GL042951

Solheim, F. S., Vivekanandan, J., Ware, R. H., & Rocken, C. (1999). Propagation delays induced in GPS signals by dry air, water vapor, hydrometeors, and other particulates. *Journal of Geophysical Research*, *104*(D8), 9663–9670. https://doi.org/10.1029/1999JD900095

Sturkell, E., Einarsson, P., Sigmundsson, F., Hreinsdóttir, S., & Geirsson, H. (2003). Deformation of Grímsvötn volcano, Iceland: 1998 eruption and subsequent inflation. *Geophysical Research Letters*, *30*(4), 1182. https://doi.org/10.1029/2002GL016460

Van Eaton, A. R., Mastin, L. G., Herzog, M., Schwaiger, H. F., Schneider, D. J., Wallace, K. L., & Clarke, A. B. (2015). Hail formation triggers rapid ash aggregation in volcanic plumes. *Nature Communications*, *6*, 7860. https://doi.org/10.1038/ncomms8860

Webley, P. W., Lopez, T. M., Ekstrand, A. L., Dean, K. G., Rinkleff, P., Dehn, J., et al. (2013). Remote observations of eruptive clouds and surface thermal activity during the 2009 eruption of Redoubt volcano. *Journal of Volcanology and Geothermal Research: Atmospheres*, *259*, 185–200. https://doi.org/10.1016/j.jvolgeores.2012.06.023

Wen, S., & Rose, W. I. (1994). Retrieval of sizes and total masses of particles in volcanic clouds using AVHRR bands 4 and 5. *Journal of Geophysical Research*, *99*(D3), 5421–5431. https://doi.org/10.1029/93JD03340

Wessel, P., & Smith, W. H. F. (1995). New version of the Generic Mapping Tools released. *Eos, Transactions American Geophysical Union*, *76*(33), 329. https://doi.org/10.1029/95EO00198

Zumberge, J. F., Heflin, M. B., Jefferson, D. C., Watkins, M. M., & Webb, F. H. (1997). Precise point positioning for the efficient and robust analysis of GPS data from large networks. *Journal of Geophysical Research*, *102*(B3), 5005–5017. https://doi.org/10.1029/96JB03860